Eur. J. Mineral., 35, 81–94, 2023
https://doi.org/10.5194/ejm-35-81-2023

European Journal of Mineralogy
Open Access

Dutrowite, $Na(Fe^{2+}_{2.5}Ti_{0.5})Al_6(Si_6O_{18})(BO_3)_3(OH)_3O$, a new mineral from the Apuan Alps (Tuscany, Italy): the first member of the tourmaline supergroup with Ti as a species-forming chemical constituent

Cristian Biagioni[1], Ferdinando Bosi[2], Daniela Mauro[1,3], Henrik Skogby[4], Andrea Dini[5], and Federica Zaccarini[6]

[1]Dipartimento di Scienze della Terra, Università di Pisa, Via Santa Maria 53, 56126 Pisa, Italy
[2]Dipartimento di Scienze della Terra, Sapienza Università di Roma, Piazzale Aldo Moro 5, 00185 Rome, Italy
[3]Museo di Storia Naturale, Università di Pisa, Via Roma 79, 56011 Calci, Italy
[4]Department of Geosciences, Swedish Museum of Natural History, P.O. Box 50007, 10405 Stockholm, Sweden
[5]Istituto di Geoscienze e Georisorse, CNR-Pisa, Via Moruzzi 1, 56124 Pisa, Italy
[6]Department of Applied Geological Sciences and Geophysics, University of Leoben, Peter Tunner Str. 5, 8700 Leoben, Austria

Correspondence: Cristian Biagioni (cristian.biagioni@unipi.it)

Received: 10 November 2022 – Revised: 17 January 2023 – Accepted: 28 January 2023 – Published: 10 February 2023

Abstract. The new tourmaline supergroup mineral dutrowite, $Na(Fe^{2+}_{2.5}Ti_{0.5})Al_6(Si_6O_{18})(BO_3)_3(OH)_3O$, has been discovered in an outcrop of a Permian metarhyolite near the hamlet of Fornovolasco, Apuan Alps, Tuscany, Italy. It occurs as chemically homogeneous domains, up to 0.5 mm, brown in colour, with a light-brown streak and a vitreous lustre, within anhedral to subhedral prismatic crystals, up to 1 mm in size, closely associated with Fe-rich oxy-dravite. Dutrowite is trigonal, space group $R3m$, with $a = 15.9864(8)$, $c = 7.2187(4)$ Å, $V = 1597.68(18)$ Å^3, and $Z = 3$. The crystal structure was refined to $R_1 = 0.0257$ for 1095 unique reflections with $F_o > 4\sigma$ (F_o) and 94 refined parameters. Electron microprobe analysis, coupled with Mössbauer spectroscopy, resulted in the empirical structural formula $^{X}(Na_{0.81}Ca_{0.20}K_{0.01})_{\Sigma 1.02}$ $^{Y}(Fe^{2+}_{1.25}Mg_{0.76}Ti_{0.56}Al_{0.42})_{\Sigma 3.00}$ $^{Z}(Al_{4.71}Fe^{3+}_{0.27}V^{3+}_{0.02}Mg_{0.82}Fe^{2+}_{0.18})_{\Sigma 6.00}$ $^{T}[(Si_{5.82}Al_{0.18})_{\Sigma 6.00}O_{18}]$ $(BO_3)^{O(3)}_3(OH)^{O(1)}_3[O_{0.59}(OH)_{0.41}]_{\Sigma 1.00}$, which was recast in the empirical ordered formula, required for classification purposes: $^{X}(Na_{0.81}Ca_{0.20}K_{0.01})_{\Sigma 1.02}$ $^{Y}(Fe^{2+}_{1.43}Mg_{1.00}Ti_{0.56})_{\Sigma 3.00}$ $^{Z}(Al_{5.13}Fe^{3+}_{0.27}V^{3+}_{0.02}Mg_{0.58})_{\Sigma 6.00}$ $^{T}[(Si_{5.82}Al_{0.18})_{\Sigma 6.00}O_{18}]$ $(BO_3)^{V}_3(OH)_3$ $^{W}[O_{0.59}(OH)_{0.41}]_{\Sigma 1.00}$. Dutrowite is an oxy-species belonging to the alkali group of the tourmaline supergroup. Titanium is hosted in octahedral coordination, and its incorporation is probably due to the substitution $2Al^{3+} = Ti^{4+} + (Fe,Mg)^{2+}$. Its occurrence seems to be related to late-stage high-T/low-P replacement of "biotite" during the late-magmatic/hydrothermal evolution of the Permian metarhyolite.

1 Introduction

The mineralogy of the Apuan Alps (Tuscany, Italy) has been studied for more than 150 years, leading to the identification of more than 300 different mineral species, among which 44 have here their type locality (Table 1). The first new mineral species to be discovered was the Cu–Pb sulfosalt meneghinite, described by Bechi (1852) from the Pb–Zn–Ag ore deposit exploited at the Bottino mine. Since then, another 24 minerals belonging to this mineral group have been identified following the mineralogical studies done on the small hydrothermal ore deposits occurring in the Apuan Alps. In these same localities, new oxide minerals were discovered, as well as a suite of secondary species related to the alteration of primary sulfides (mainly pyrite – e.g. Biagioni et al., 2020). Conversely, silicate minerals associated with these ore deposits were usually neglected, the only exception being allanite-(La) by Orlandi and Pasero (2006). It is worth noting that several ore deposits embedded in the Paleozoic basement of the Apuan Alps are spatially associated with tourmalinite bodies (e.g. Benvenuti et al., 1989) and tourmaline-bearing Permian metarhyolite rocks (Vezzoni et al., 2018). However, few data on tourmaline supergroup minerals from the Apuan Alps are available (Benvenuti et al., 1991; Mauro et al., 2022).

In the framework of an ongoing study of the crystal chemistry of non-pegmatitic tourmaline supergroup minerals from Tuscany (Italy), tourmaline samples from Permian metarhyolite exposed in the Fornovolasco area (southern Apuan Alps) were studied. Preliminary chemical analyses indicated the occurrence of a Ti-rich tourmaline supergroup mineral deserving additional investigations. Further studies confirmed the preliminary results, and the mineral dutrowite, as well as its name, were approved by the Commission on New Minerals, Nomenclature and Classification of the International Mineralogical Association (CNMNC-IMA) under voting number 2019-082. The name honours Barbara Lee Dutrow (born 1956), Adolphe G. Gueymard professor at Louisiana State University, for her contributions to the understanding of the chemical variability of tourmaline supergroup minerals, as well as on the petrologic significance of staurolite. Holotype material is deposited in the mineralogical collection of the Museo di Storia Naturale, University of Pisa, Via Roma 79, Calci (Pisa), under catalogue number 19890.

This paper describes the new mineral species dutrowite, discussing its crystal chemistry and its possible petrologic significance.

2 Occurrence and physical properties

Dutrowite was identified in a sample from the outcrop of the Fornovolasco Metarhyolite Formation (Pieruccioni et al., 2018) close to the Boscaccio locality (44°01′53″ N, 10°22′11″ E), near the small hamlet of Fornovolasco, Fabbriche di Vergemoli, Apuan Alps, Tuscany, Italy. The Fornovolasco Metarhyolite Formation is represented by lenticular bodies of usually massive porphyritic, tourmaline-bearing metarhyolite embedded in Paleozoic phyllites belonging to the Lower Phyllites Fm., having an early Cambrian depositional age (Paoli et al., 2017). Radiometric U–Pb dating on zircon suggested a Permian crystallization age for the metarhyolite bodies (Vezzoni et al., 2018). The first petrographic description of these rocks was reported by Bonatti (1933), who also described the occurrence of tourmaline supergroup minerals, characterized by a pleochroism with ω = light blue and ε = light yellow to colourless. Tourmaline, intergrown with quartz, occurs as rounded millimetre-to-centimetre-sized orbicules that are wrapped and locally cut by the metamorphic foliation as well as small irregular patches dispersed in the groundmass. The tourmaline orbicules represent a primary feature of the Permian magmatic rock, clearly indicating its subvolcanic intrusive origin.

Dutrowite was found as chemically homogeneous domains within anhedral to subhedral crystals up to 1 mm in size (Fig. 1); domains of dutrowite can reach up to 0.5 mm across. Colour is brown, with a light-brown streak. Dutrowite is transparent, with a vitreous lustre. It is brittle, with an irregular fracture. Hardness was not measured, but it should be about 7–7.5, by analogy with other members of the tourmaline supergroup. Calculated density, based on the empirical formula and unit-cell parameters from single-crystal X-ray diffraction, is 3.203 g cm^{-3}. In thin section, dutrowite is transparent and pleochroic, with ω = dark brown and ε = light brown. It is uniaxial (–). Refractive indices were not measured; the mean refractive index, calculated according to the Gladstone–Dale relation (Mandarino, 1979, 1981), is 1.800. It is worth noting that, as the chemical composition of tourmaline supergroup minerals is very complex, it is unrealistic to unambiguously identify a member of this supergroup on the basis of its optical properties, in agreement with other chemically complex group of minerals (e.g. allanite group – Armbruster et al., 2006).

In type material, dutrowite is associated with quartz, altered feldspars (both albite and K-feldspar), Mg-rich annite (hereafter "biotite"), Fe-rich clinochlore, muscovite, and minor "apatite", ilmenite, rutile and zircon. Moreover, it is associated with domains of Fe-rich oxy-dravite.

3 Experiment

3.1 Raman spectroscopy

Micro-Raman spectra were obtained on the sample of dutrowite shown in Fig. 1 in nearly back-scattered geometry with a Jobin-Yvon Horiba XploRA Plus apparatus, equipped with a motorized x–y stage and an Olympus BX41 microscope with a 100× objective (Dipartimento di Scienze della

Table 1. New mineral species from the Apuan Alps (Tuscany, Italy).

Mineral species	Type locality	Mineral species	Type locality
Sulfides and sulfosalts			
Andreadiniite	Monte Arsiccio mine	Meneghinite	Bottino mine
Arsenmarcobaldiite	Verzalla	Moëloite	Seravezza
Arsiccioite	Monte Arsiccio mine	Parasterryite	Pollone mine
Bernarlottiite	Seravezza	Pellouxite	Buca della Vena mine
Boscardinite	Monte Arsiccio mine	Pillaite	Buca della Vena mine
Carducciite	Pollone mine	Polloneite	Pollone mine
Disulfodadsonite	Seravezza	Protochabournéite	Monte Arsiccio mine
Garavellite	Frigido mine	Pyradoketosite	Monte Arsiccio mine
Grumiplucite	Levigliani mine	Rouxelite	Buca della Vena mine
Kenoargentotennantite-(Fe)	Pollone mine	Scainiite	Buca della Vena mine
Marcobaldiite	Pollone mine	Tetrahedrite-(Fe)	Frigido mine
Marrucciite	Buca della Vena mine	Tetrahedrite-(Hg)	Buca della Vena mine
Meerschautite	Pollone mine		
Oxides			
Apuanite	Buca della Vena mine	Mapiquiroite	Monte Arsiccio mine/ Buca della Vena mine
Bianchiniite	Monte Arsiccio mine	Oxycalcioroméite	Buca della Vena mine
Bottinoite	Bottino mine	Versiliaite	Buca della Vena mine
Dessauite-(Y)	Buca della Vena mine	Zincalstibite	Carrara
Carbonates			
Zaccagnaite	Carrara		
Sulfates			
Carraraite	Carrara	Scordariite	Monte Arsiccio mine
Giacovazzoite	Monte Arsiccio mine	Volaschioite	Fornovolasco mine
Magnanelliite	Monte Arsiccio mine		
Phosphates			
Bohuslavite	Buca della Vena mine		
Silicates			
Allanite-(La)	Buca della Vena mine	Scorticoite	Scortico-Ravazzone
Dutrowite	Fornovolasco	Suenoite	Scortico-Ravazzone

Terra, Università di Pisa). The 532 nm line of a solid-state laser was used. The minimum lateral and depth resolution was set to a few micrometres. The system was calibrated using the 520.6 cm^{-1} Raman band of silicon before each experimental session. Spectra were collected through multiple acquisitions with single counting times of 120 s, with the unfiltered laser power (25 mW). Backscattered radiation was analysed with a 1200 g mm^{-1} grating monochromator.

3.2 Chemical data and Mössbauer spectroscopy

Quantitative chemical analyses of dutrowite and associated oxy-dravite were done using a Superprobe JEOL JXA 8200 electron microprobe (WDS mode, 15 kV, 10 nA, 1 µm beam diameter) at the Eugen F. Stumpfl laboratory, Leoben University (Austria) (Table 2). Natural and synthetic standards (element, emission line) were rhodonite (Si$K\alpha$, Mn$K\alpha$), ilmenite (Ti$K\alpha$), sanidine (Al$K\alpha$, K$K\alpha$), vanadium (V$K\alpha$), olivine (Fe$K\alpha$, Mg$K\alpha$), wollastonite (Ca$K\alpha$) and albite (Na$K\alpha$). Fluorine was sought but was below the detection limit. Boron content was assumed to be stoichiometric (B = 3 atoms per formula unit, apfu) in accord with the structural information. In agreement with Pesquera et al. (2016), Li was considered negligible as MgO contents > 2 wt %. The (OH) content was finally calculated by charge balance, with the assumption $T + Y + Z = 15$ apfu and [O + (OH)] = 31 apfu. X-ray maps of the studied crystals were collected using the same analytical conditions.

The Fe^{2+}/Fe^{3+} ratio was determined by Mössbauer spectroscopy. However, owing to the small amount of homoge-

Table 2. Chemical data (in wt %) for dutrowite and associated oxy-dravite.

Constituent	Dutrowite			Oxy-dravite		
	Mean ($n = 10$)	Range	SD (σ)	Mean ($n = 135$)	Range	SD (σ)
SiO_2	34.38	33.86–34.77	0.32	37.17	35.28–38.79	0.58
TiO_2	4.40	2.78–5.65	0.88	0.36	0.09–1.92	0.26
$B_2O_{3(calc)}$	10.26			10.65		
Al_2O_3	26.63	24.69–28.69	1.35	32.30	28.82–35.30	1.33
V_2O_3	0.17	0.12–0.22	0.03	0.02	0.00–0.12	0.02
MgO	6.25	5.79–6.52	0.21	5.45	4.55–6.38	0.36
CaO	1.08	0.76–1.51	0.23	0.80	0.24–1.65	0.28
MnO	0.03	0.01–0.05	0.01	0.02	0.00–0.08	0.02
FeO_{tot}	11.99	11.18–12.85	0.58			
Fe_2O_3*	2.11			8.28		
FeO*	10.10			1.75		
Na_2O	2.46	2.26–2.71	0.12	2.09	1.77–2.67	0.16
K_2O	0.06	0.05–0.07	0.01	0.05	0.00–0.27	0.05
H_2O_{calc}	3.01			3.12		
Total	100.93					

Note: n: number of spot analyses. * Calculated according to Mössbauer data.

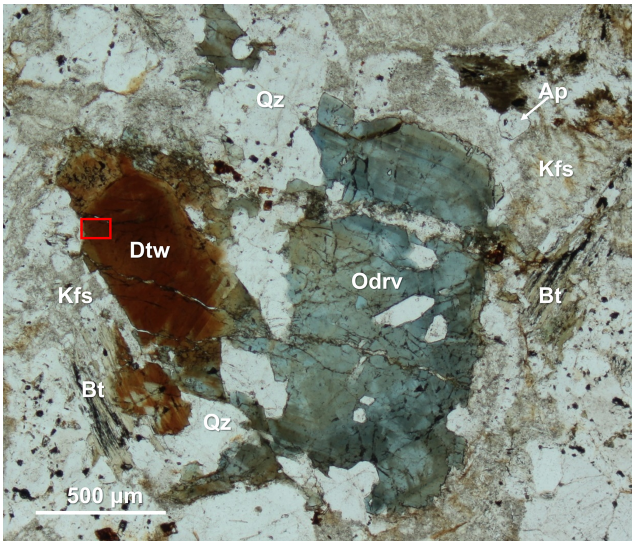

Figure 1. Photomicrograph of dutrowite in plane-polarized light. Symbols after Warr (2021): Ap – "apatite"; Bt – "biotite"; Dtw – dutrowite; Kfs – K-feldspar; Odrv – oxy-dravite; Qz – quartz. "Biotite" is partially altered in "chlorite" and rutile, whereas K-feldspar is sericitized. Red box corresponds to the area where the grain used for single-crystal X-ray diffraction was extracted. Type material. Catalogue number 19890, Museo di Storia Naturale, Università di Pisa.

neous material, Mössbauer data were collected on several grains of tourmaline separated from the groundmass and the tourmaline orbicules occurring in the metarhyolite. Consequently, the obtained values can be considered as a grand value of tourmaline species with similar Mg and Fe contents

Table 3. Mössbauer parameters for tourmaline (dutrowite and associated oxy-dravite) collected at room temperature.

δ (mm s^{-1})	ΔE_Q (mm s^{-1})	FWHM (mm s^{-1})	I (%)	Assignment
1.08	2.38	0.24	29.8	$^{VI}Fe^{2+}$
1.09	2.58	0.22	19.0	$^{VI}Fe^{2+}$
1.06	2.04	0.31	16.9	$^{VI}Fe^{2+}$
1.04	1.61	0.46	18.5	$^{VI}Fe^{2+}$
0.53	0.69	0.64	15.8	$^{VI}Fe^{3+}$

δ: centroid shift, ΔE_Q: quadrupole splitting, FWHM: full width at half-maximum.

and different Ti and Al contents (see Vezzoni et al., 2018). The Mössbauer spectrum was collected at room temperature in transmission mode using a ^{57}Co source in Rh matrix with a nominal activity of 50 mCi. It was acquired over the velocity range ± 4 mm s^{-1} and was calibrated against α-Fe foil. The spectrum could be adequately fitted with four quadrupole doublets assigned to Fe^{2+} and one doublet assigned to Fe^{3+} using the program MossA (Prescher et al., 2012) (Table 3).

3.3 X-ray crystallography

Intensity data were collected using a Bruker Apex II diffractometer equipped with a Photon II CCD area detector and graphite-monochromatized Mo$K\alpha$ radiation. The detector-to-crystal distance was 50 mm. A total of 983 frames were collected using ω and φ scan modes, in 0.5° slices, with an exposure time of 40 s per frame. The data were corrected for Lorentz and polarization factors and absorption using

the software package Apex3 (Bruker AXS Inc., 2016). The crystal structure of dutrowite was refined using Shelxl 2018 (Sheldrick, 2015). Starting atom coordinates were taken from Bosi and Skogby (2013). The statistical tests on the distribution of $|E|$ values and the systematic absences agree with the space group $R3m$. The following neutral scattering curves, taken from the *International Tables for Crystallography* (Wilson, 1992), were used: Na vs. Ca at X, Mg vs. Fe at Y, and Al vs. Fe at Z. The T and B sites were modelled, respectively, with Si and B scattering factors and with a fixed occupancy of 1, because refinement with unconstrained occupancies showed no significant deviations from this value. The H(3) and O sites were assumed to be fully occupied by H and O, respectively. Fully ionized scattering curves were used for oxygen atoms. The isotropic displacement parameter of $^{H(3)}$H atom was assumed to be 1.2 times of the U_{eq} value of the $^{O(3)}$O atom to which it is bonded. An anisotropic structural model converged to $R_1 = 0.026$ for 1095 unique reflections with $F_o > 4\sigma\ (F_o)$ and 94 refined parameters. Details of data collection and refinement are given in Table 4.

4 Results and discussion

4.1 Raman spectrum of dutrowite

The micro-Raman spectrum of dutrowite is displayed in Fig. 2. The Raman shift of the observed bands is shown, as obtained through fit profile using Fityk (Wojdyr, 2010). In the region between 100 and 1200 cm^{-1} (Fig. 2a, b), vibrational modes of YO_6 (in the range $\sim$200–240 cm^{-1}), ZO_6 (range 360–375 cm^{-1}), SiO_4 rings vibrations (between $\sim$650 and 720 cm^{-1}), BO_3 bending and stretching modes (in the range 730–780 cm^{-1}), and SiO_4 stretching modes (between 760 and 1120 cm^{-1}) occur, in agreement with previous authors (e.g. Gasharova et al., 1997; Watenphul et al., 2016a, b). The stretching of O–H bonds occurs in the region between 3400 and 3800 cm^{-1} (Fig. 2c).

Watenphul et al. (2016a, b) discussed the relations between band positions and crystal chemistry of the studied tourmalines. In particular, the vibrational modes of YO_6 and ZO_6 polyhedra are sensitive to the Mg contents and Fe contents, as well as to the Fe oxidation state (Watenphul et al., 2016b); similarly, the short-range cation distribution around the O(1) and O(3) sites affects the band positions in the O–H stretching region (Gonzalez-Carreño et al., 1988; Bosi et al., 2015; Watenphul et al., 2016a). Specifically, the band at about 3565 cm^{-1} is related to O(3), whereas the less-intense band at about 3636 cm^{-1} is related to O(1). The latter is consistent with the reduced content of $^{O(1)}(OH)_{0.41}$ (see below).

4.2 Chemical formula and crystallography of dutrowite

Fractional atom coordinates and displacement parameters of dutrowite are reported in Table 5, and selected bond distances are given in Table 6. Following Henry et al. (2011), the empirical ordered formula of dutrowite is $^{X}(Na_{0.81}Ca_{0.20}K_{0.01})_{\Sigma 1.02}\ ^{Y}(Fe^{2+}_{1.43}Mg_{1.00}Ti_{0.56})_{\Sigma 3.00}\ ^{Z}(Al_{5.13}Fe^{3+}_{0.27}V^{3+}_{0.02}Mg_{0.58})_{\Sigma 6.00}\ ^{T}[(Si_{5.82}Al_{0.18})_{\Sigma 6.00}O_{18}](BO_3)^{V}_{3}\ (OH)_3\ ^{W}[O_{0.59}(OH)_{0.41}]_{\Sigma 1.00}$. This formula, useful for classification purposes, indicates that dutrowite belongs to a new subgroup, having $Y = R^{2+}_{2.5}R^{4+}_{0.5}$ and $Z = R^{3+}_{6}$, within the alkali group. Oxygen is dominant at W, thus indicating that dutrowite is an oxy-member of the tourmaline supergroup. The distribution of Fe^{2+} and Fe^{3+} is in keeping with the results of Mössbauer spectroscopy (Fig. 3), which are consistent with Fe^{2+} at the Y position and Fe^{3+} in the Z position (e.g. Andreozzi et al., 2008), although a unique Fe site distribution cannot be achieved due to the unresolved absorption doublets.

The empirical structural formula of dutrowite was optimized using the method of Wright et al. (2000), distributing cations among the Y, Z, and T sites as follows: $^{X}(Na_{0.81}Ca_{0.20}K_{0.01})_{\Sigma 1.02}\ ^{Y}(Fe^{2+}_{1.25}Mg_{0.76}Ti_{0.56}Al_{0.42})_{\Sigma 3.00}\ ^{Z}(Al_{4.71}Fe^{3+}_{0.27}V^{3+}_{0.02}Mg_{0.82}Fe^{2+}_{0.18})_{\Sigma 6.00}\ ^{T}[(Si_{5.82}Al_{0.18})_{\Sigma 6.00}O_{18}]\ (BO_3)^{O(3)}_{3}(OH)^{O(1)}_{3}[O_{0.59}(OH)_{0.41}]_{\Sigma 1.00}$. Both empirical formulae lead to the end-member composition $Na(Fe^{2+}_{2.5}Ti_{0.5})Al_6(Si_6O_{18})(BO_3)_3(OH)_3O$, corresponding to (in wt %) SiO_2 34.38, TiO_2 3.81, B_2O_3 9.96, Al_2O_3 29.18, FeO 17.13, Na_2O 2.96, H_2O 2.58, total 100.00.

Table 7 compares the site scattering and the proposed site populations. Bond-valence calculations, weighted according to the optimized site populations and obtained using the bond-valence parameters of Brese and O'Keeffe (1991), are reported in Table 8. There is an excellent match between observed and refined site scattering, i.e. 142.63 vs. 142.20 electrons per formula unit, respectively. Moreover, the ^{W}(OH) content (0.41 apfu) is in good agreement with that calculated using the equation reported by Bosi (2013): $^{W}(OH) = \{2 - 1.01 \times BVS[O(1)] - 0.21 - F\} = 0.40$ apfu, where BVS[O(1)] is the bond-valence sum at the O(1) site (Table 8).

Owing to the small size of the available material, no X-ray powder diffraction pattern of dutrowite was collected. The calculated X-ray powder diffraction pattern, based on the structural model given in Table 5, is reported in Table 9.

4.3 Titanium in tourmaline supergroup minerals and crystal chemistry of dutrowite

Dutrowite is the first tourmaline supergroup mineral having Ti ($Z = 22$) as a species-forming chemical constituent, although the occurrence of this element in these cyclosilicates as a minor component is well-known. Titanium-bearing tourmalines are known from several geological environments, and some authors have considered this element a geochemical proxy for unveiling the genesis of the studied assemblages; for instance, Ribeiro da Costa et al. (2021) suggested that Ti can be used for discriminating between evolved and less evolved granitic rocks, the latter being usually richer in Ti than the former.

Table 4. Summary of parameters describing data collection and refinement for dutrowite.

Crystal data	
Crystal size (mm)	$0.080 \times 0.037 \times 0.030$
Space group	$R3m$
a (Å)	15.9864(8)
c (Å)	7.2187(4)
V (Å^3)	1597.68(18)
Z	3
Data collection and refinement	
Radiation, wavelength (Å)	Mo $K\alpha$, 0.71073
Temperature (K)	293(2)
$2\theta_{max}$ (°)	59.98
Measured reflections	7319
Unique reflections	1145
Reflections with $F_o > 4\sigma\ (F_o)$	1095
R_{int}	0.0441
$R\sigma$	0.0327
Range of h, k, l	$-22 \le h \le 20, -17 \le k \le 22, -10 \le l \le 10$
$R_1\ [F_o > 4\sigma\ (F_o)]$	0.0257
R_1(all data)	0.0290
wR_2 (on F_o^2)[a]	0.0457
Goof	1.137
Flack parameter[b]	0.18(4)
Number of least-squares parameters	94
Maximum and minimum residual peak (e Å^{-3})	0.47 [at 1.56 Å from X] −0.42 [at 1.33 Å from B]

[a] $w = 1/[\sigma^2(F_o^2) + (0.0043P)^2 + 3.6400P]$. [b] Flack (1983).

Table 5. Sites, Wyckoff positions, site occupancies (s.o.), fractional atom coordinates, and isotropic (*) or equivalent isotropic displacement parameters (in Å^2) for dutrowite.

Site	Wyckoff position	s.o.	x/a	y/b	z/c	$U_{eq/iso}$
X	3a	$Na_{0.79(1)}Ca_{0.21(1)}$	0	0	0.2261(5)	0.0222(14)
Y	9b	$Fe_{0.56(1)}Mg_{0.44(1)}$	0.12384(8)	0.06192(4)	0.6339(2)	0.0104(3)
Z	18c	$Al_{0.94(1)}Fe_{0.06(1)}$	0.29846(8)	0.26189(8)	0.6113(2)	0.0079(3)
B	9b	$B_{1.00}$	0.1105(2)	0.2210(5)	0.4537(9)	0.0107(11)
T	18c	$Si_{1.00}$	0.19173(7)	0.18988(7)	0	0.0070(2)
O(1)	3a	$O_{1.00}$	0	0	0.7818(11)	0.0229(17)
O(2)	9b	$O_{1.00}$	0.06112(14)	0.1222(3)	0.4815(5)	0.0132(8)
O(3)	9b	$O_{1.00}$	0.2665(3)	0.13327(15)	0.5115(5)	0.0130(8)
H(3)	9b	$H_{1.00}$	0.257(5)	0.129(2)	0.380(4)	0.01558*
O(4)	9b	$O_{1.00}$	0.09235(14)	0.1847(3)	0.0710(5)	0.0125(8)
O(5)	9b	$O_{1.00}$	0.1841(3)	0.09206(14)	0.0896(5)	0.0110(8)
O(6)	18c	$O_{1.00}$	0.19608(19)	0.18670(19)	0.7785(4)	0.0097(5)
O(7)	18c	$O_{1.00}$	0.28443(18)	0.28402(17)	0.0791(4)	0.0099(6)
O(8)	18c	$O_{1.00}$	0.20944(19)	0.2701(2)	0.4412(4)	0.0119(6)

Henry and Dutrow (1996), reviewing the contents of minor chemical constituents in tourmaline supergroup minerals, reported up to 4.07 wt % TiO_2; this content was given by Lottermoser and Plimer (1987) for dravite occurring within contact rocks in a breccia diatreme at Umberatana, South Australia. Grice and Ercit (1993) reported data for two tourmalines having 2.87 wt % and 2.19 wt % TiO_2; these values correspond to 0.40 and 0.29 Ti apfu, respectively. Still higher TiO_2 contents, 4.70 wt %, were later measured in a bosiite-like tourmaline by Flégr et al. (2016); this weight percent

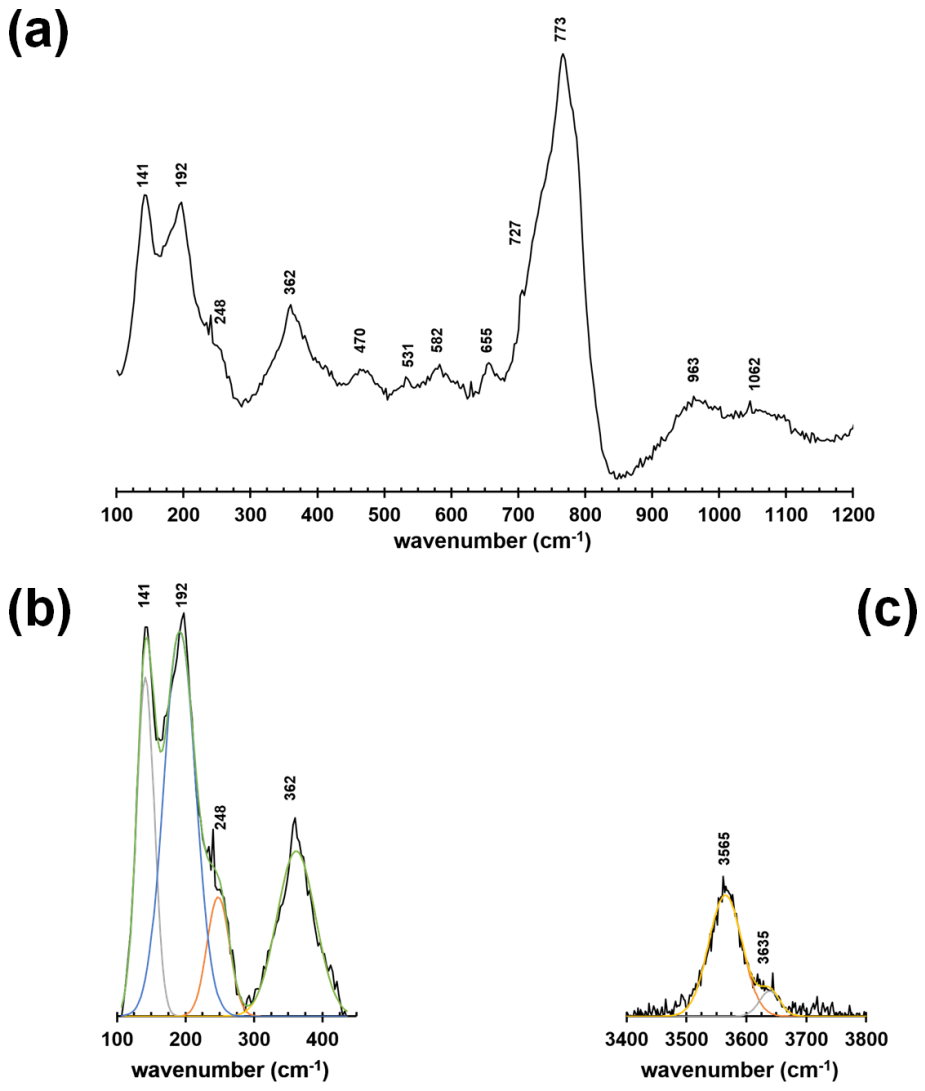

Figure 2. Raman spectrum of dutrowite **(a)** and fitting of the spectral region between 100 and 500 cm^{-1} **(b)** and 3400–3800 cm^{-1} **(c)**.

value corresponds to 0.64 Ti apfu. Scribner et al. (2018) found 0.26 and 0.28 Ti apfu in Ca-rich tourmaline from the O'Grady batholith, Northwest Territories, Canada.

Titanium-rich tourmaline supergroup minerals have been identified in the Třebíč pegmatites, Manjaka and Řečice, in the Czech Republic, with Ti contents up to 0.55, 0.59, and 0.64 apfu, respectively (Novák et al., 2011; Gadas et al., 2019). Konzett et al. (2012) measured up to 3.42 wt % TiO_2 in tourmaline from (Fe,Ti)-rich eclogite from the Kreuzeck Mountains, Eastern Alps, Austria.

Titanium was reported by Dutrow and Henry (2022) in tourmaline from an (anhydrite–gypsum)-bearing meta-evaporite sampled in the Arignac Gypsum Mine, France; one spot analysis, having $Ti > 0.25$ apfu and $^{Y}Ti > {}^{Y}Al$, is consistent with hypothetical "magnesio-dutrowite", with empirical ordered formula $^{X}(Na_{0.64}Ca_{0.31}\square_{0.05})_{\Sigma 1.00}$ $^{Y}(Mg_{2.71}Ti_{0.29})_{\Sigma 3.00}$ $^{Z}(Al_{5.56}Fe^{3+}_{0.18}Mg_{0.26})_{\Sigma 6.00}$ $[(Si_{5.93}Al_{0.07})_{\Sigma 6.00}O_{18}]$ $(BO_3)^{V}_{3}(OH)_3$ $^{W}[O_{0.50}(OH)_{0.49}F_{0.01}]_{\Sigma 1.00}$. High-Ti contents (up to 0.56 apfu) in tourmaline from meta-evaporites were previously reported by Žáček et al. (2000) from Bolivia. Another possible occurrence of "magnesio-dutrowite" is reported by Bačík et al. (2022) in tourmalinites from Zlatá Idka, Slovakia; these authors found Ti contents up to 0.38 apfu, and they identified two distinct compositional trends, i.e. schorl–dutrowite and dravite–"magnesio-dutrowite".

Several substitution mechanisms have been proposed to explain the occurrence of Ti in the crystal structure of tourmaline supergroup minerals. Some authors have argued the Ti substitution at the *T* site (e.g. Povondra, 1981; Grice and Ercit, 1993), but this statement is not supported by optical spectra (Rossman and Mattson, 1986). In addition, the crystal structure refinement of dutrowite does not

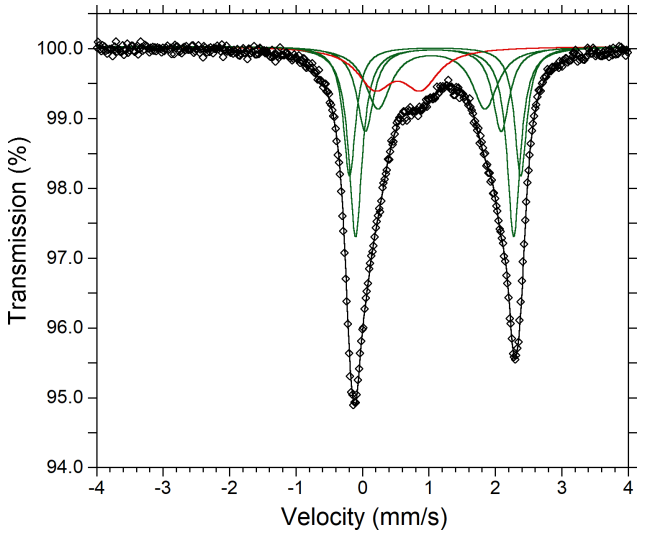

Figure 3. Mössbauer spectrum of tourmaline supergroup minerals (dutrowite and associated oxy-dravite). Fitted absorption doubled assigned to Fe^{2+} and Fe^{3+} are indicated in green and red colours, respectively. Diamonds denote measured spectrum, and the black curve represents summed fitted spectra.

Table 6. Selected bond distances (in Å) for dutrowite.

X	–O(2)	2.503(4) × 3	*Y*	–O(1)	2.020(4)
	–O(5)	2.733(4) × 3		–O(6)	2.024(3) × 2
	–O(4)	2.791(4) × 3		–O(2)	2.028(3) × 2
	mean	**2.676**		–O(3)	2.164(4)
				mean	**2.048**
Z	–O(8)	1.899(3)			
	–O(6)	1.901(3)	*B*	–O(8)	1.373(4) × 2
	–O(7)	1.909(3)		–O(2)	1.382(8)
	–O(8)	1.933(3)		**mean**	**1.376**
	–O(7)	1.972(3)			
	–O(3)	1.9895(19)	*T*	–O(7)	1.599(2)
	mean	**1.934**		–O(6)	1.602(3)
				–O(4)	1.6316(16)
				–O(5)	1.6398(18)
				mean	**1.618**

agree with the occurrence of tetrahedrally coordinated Ti. Consequently, Ti occurs in octahedral coordination, but its assignment to the *Y* or *Z* site is ambiguous even from a theoretical viewpoint (see Appendix 1 in Bosi and Andreozzi, 2013). Gadas et al. (2019) reported the possible substitution $Ca^{2+} + 2Ti^{4+} + 2Mg^{2+} + O^{2-} = Na^{+} + 4Al^{3+} + (OH)^{-}$ for tourmaline from Manjaka, whereas in Ca-poor tourmaline from Řečice Ti seems to be incorporated through the substitution $Ti^{4+} + O^{2-} = Al^{3+} + (OH)^{-}$. Nabelek (2021) proposed the substitution mechanism $2Na^{+} + (Fe,Mg)^{2+} + 2(OH)^{-} = Ca^{2+} + \square + Ti^{4+} + O^{2-}$, also observing a negative correlation between Ti and Al, for tourmalines from tourmalinites in South Dakota, USA. At

Table 7. Refined and calculated site-scattering (s.s., in electrons per formula unit) and proposed site population (in atoms per formula unit) for dutrowite.

Site	Refined s.s.	Proposed site population	Calculated s.s.
X	12.89	$Na_{0.80}Ca_{0.20}$	12.80
Y	59.52	$Fe^{2+}_{1.25}Mg_{0.76}Ti_{0.56}Al_{0.42}$	59.40
Z	82.68	$Al_{4.71}Fe^{3+}_{0.27}V_{0.02}Mg_{0.82}Fe^{2+}_{0.18}$	83.23
Σ (*Y* + *Z*)	142.20		142.63
T	84.00	$Si_{5.82}Al_{0.18}$	83.82
B	5.00	$B_{3.00}$	5.00

Fornovolasco, where dutrowite was discovered, Vezzoni et al. (2018) pointed out the variability of the crystal chemistry of tourmaline by a wide range of Fe/(Fe + Mg) ratios, as well as by different degrees of Al saturation. Moreover, these authors suggested a positive correlation between the content of Ti and (Mg + Fe) and a negative relation with the Al content, which results in the heterovalent substitution $2Al^{3+} = Ti^{4+} + (Fe,Mg)^{2+}$.

In addition to chemical data reported in Table 1, collected on the area where the grain of dutrowite used for the single-crystal X-ray diffraction study was extracted, other spot analyses were done on the other domains having brown and blue absorption colours in transmitted light microscopy (Fig. 1), respectively. All spot analysis data are deposited in the Supplement. Brown domains are usually enriched in Ti, in agreement with previous results obtained, for instance by da Fonseca-Zang et al. (2008). The blue domain, whose average chemical composition is given in Table 2, has the following empirical ordered formula: $^{X}(Na_{0.66}Ca_{0.14}K_{0.01})_{\Sigma 0.81}$ $^{Y}(Mg_{1.33}Fe^{2+}_{1.13}Al_{0.42}Ti_{0.04})_{\Sigma 2.92}$ $^{Z}(Al_{5.79}Fe^{3+}_{0.21})_{\Sigma 6.00}$ $^{T}[Si_{6.07}O_{18}]$ $(BO_3)_3$ $^{V}(OH)_3$ $^{W}[O_{0.60}(OH)_{0.40}]_{\Sigma 1.00}$. This is another member of the alkali group that, in agreement with Bosi et al. (2019), corresponds to the end-member formula $Na(Mg_2Al)Al_6(Si_6O_{18})(BO_3)_3(OH)_3O$, which is oxy-dravite. The blue domain of this tourmaline has a $Mg/(Mg + Fe^{2+})$ atomic ratio with an average value of 0.54(2), ranging between 0.47 and 0.60. Consequently, some domains have a composition with Fe^{2+} slightly dominant over Mg and thus probably corresponding to oxy-schorl.

Figure 4 shows the X-ray maps for selected elements in dutrowite and associated oxy-dravite. Whereas Na is homogeneously distributed between these two phases, Ca is depleted in the core of the crystal; the X-ray map collected using Ca$K\alpha$ allows the identification of several anhedral to subhedral grains of "apatite". Iron and Mg are rather constant in the crystal of tourmaline, although a slight enrichment seems to occur in the domain enriched in Ti; on the contrary, Al is depleted in this latter area. X-ray maps of Fe and Mg also allow identification of "biotite", partially replaced by Fe-rich clinochlore. "Biotite" is also relatively enriched in Ti (2.70 wt % TiO_2, according to Vezzoni et al., 2018);

Table 8. Weighted bond valence (in valence units) in dutrowite.

Site	*X*	*Y*	*Z*	*T*	*B*	Σ_{anions}
O(1)		$^{3\times\rightarrow}0.46$				1.38
O(2)	$0.17^{\downarrow\times3}$	$^{2\times\rightarrow}0.45^{\downarrow\times2}$			0.97	2.04
O(3)		0.31	$^{2\times\rightarrow}0.42$			1.15
O(4)	$0.08^{\downarrow\times3}$			$^{2\times\rightarrow}0.98$		2.04
O(5)	$0.09^{\downarrow\times3}$			$^{2\times\rightarrow}0.96$		2.01
O(6)		$0.45^{\downarrow\times2}$	0.53	1.06		2.04
O(7)			0.52 0.44	1.07		2.03
O(8)			0.53 0.49		$0.99^{\downarrow\times2}$	2.01
$\Sigma_{cations}$	1.02	2.57	2.93	4.07	2.95	
Expected	1.20	2.51	2.83	4.00	3.00	

Note: left and right superscripts indicate the number of equivalent bonds involving anions and cations, respectively.

Table 9. X-ray powder diffraction data (d in Å) for dutrowite. Intensity and d_{hkl} were calculated using the software PowderCell 2.3 (Kraus and Nolze, 1996) on the basis of the structural model given in Table 5. Only the reflections with $I_{calc} > 5$ are given. The seven strongest reflections are given in bold.

I_{calc}	d_{calc}	*h k l*	I_{calc}	d_{calc}	*h k l*
42	**6.40**	**1 0 1**	7	2.134	3 0 3
17	5.00	0 2 1	11	2.061	2 2 3
18	4.61	3 0 0	**41**	**2.048**	**1 5 2**
52	**4.24**	**2 1 1**	8	2.026	1 6 1
60	**4.00**	**2 2 0**	24	1.925	3 4 2
48	**3.493**	**0 1 2**	7	1.882	1 4 3
6	3.390	1 3 1	7	1.855	6 2 1
9	3.021	4 1 0	5	1.665	6 0 3
61	**2.971**	**1 2 2**	14	1.665	0 6 3
9	2.907	3 2 1	12	1.647	2 7 1
100	**2.585**	**0 5 1**	17	1.599	5 5 0
7	2.406	0 0 3	5	1.532	7 2 2
14	2.384	2 3 2	14	1.512	0 5 4
13	2.351	5 1 1	14	1.461	5 1 4
14	2.197	5 0 2	5	1.454	6 4 2
10	2.171	4 3 1	5	1.436	7 4 0

minor Ti-rich oxides (rutile, ilmenite) can also be observed. This qualitative description is confirmed by a quantitative estimation based on electron microprobe analysis.

Chemical variability of dutrowite and associated oxy-dravite is shown in Fig. 5. In agreement with Novák et al. (2011), considering $Al_{tot} = 6$ apfu as a threshold for Al saturation, dutrowite is usually Al-undersaturated, i.e. Al < 6 apfu, whereas associated oxy-dravite is richer in Al, with Al up to 6.8 apfu. The low Al content of Ti-bearing tourmalines was also reported by Scribner et al. (2018). Dutrowite has a slightly lower Na/(Na + Ca) ratio than oxy-dravite; the lower value is not related to higher Ca content in the former, but to lower Na content in oxy-dravite, that has similar Ca contents but a higher amount of vacancy at the *X* site. Magnesium and Fe^{2+} are positively correlated in oxy-dravite and dutrowite, with Fe and Mg enriched in the latter. This behaviour is related to the negative correlation between the $(Mg + Fe^{2+})$ and Al content: dutrowite, having the highest $(Mg + Fe^{2+})$ content, is Al-undersaturated. It is worth noting that $(Mg + Fe^{2+})$ has a positive correlation with Ti^{4+}, suggesting the substitution mechanism $2Al^{3+} = Ti^{4+} + (Mg,Fe)^{2+}$. This substitution is further strengthened by the negative correlation between the contents of Ti and R^{3+} cations occurring in dutrowite, mainly represented by Al, with minor content of Fe^{3+} and V^{3+}; this agrees, for instance, with the results of Novák et al. (2011). The possible involvement of Ca^{2+} in the substitution favouring the incorporation of Ti in the crystal structure of tourmaline, suggested by some authors (e.g. Dini et al., 2008; Gadas et al., 2019), is not supported by the current data; indeed, chemical data are quite scattered, and Ca enrichment in dutrowite with respect to oxy-dravite (∼ 0.06 apfu) is low. Consequently, chemical data collected on type material of dutrowite are consistent with previous studies on both natural (e.g. Žáček et al., 2000; Konzett et al., 2012) and synthetic (Vereshchagin et al., 2022) tourmalines, indicating the substitution $2Al^{3+} = Ti^{4+} + (Mg/Fe)^{2+}$ as the most probable substitution in Ti-rich members of the tourmaline supergroup. Some previous data also indicated a decrease in the OH content and an increase in the oxy-nature of tourmalines (e.g. Gadas et al., 2019), coupled with the Ti incorporation via the substitution $Al^{3+} + (OH)^{-} = Ti^{4+} + O^{2-}$. Such a mechanism may also occur in dutrowite, possibly coupled with the other involving Mg and Fe, e.g. $3Al^{3+} + (OH)^{-} = 2Ti^{4+} + (Fe,Mg)^{2+} + O^{2-}$.

These substitution mechanisms should favour an increase in the unit-cell parameters, indeed, in agreement with the ionic radii of Shannon (1976), $r_{Mg} > r_{Ti} > r_{Al}$. Dottorini (2019) gave the crystallographic data of the tourmaline supergroup minerals occurring in the Fornovolasco Metarhyolite Formation and reported SEM-EDS data. According to these data, tourmaline can be classified as oxy-

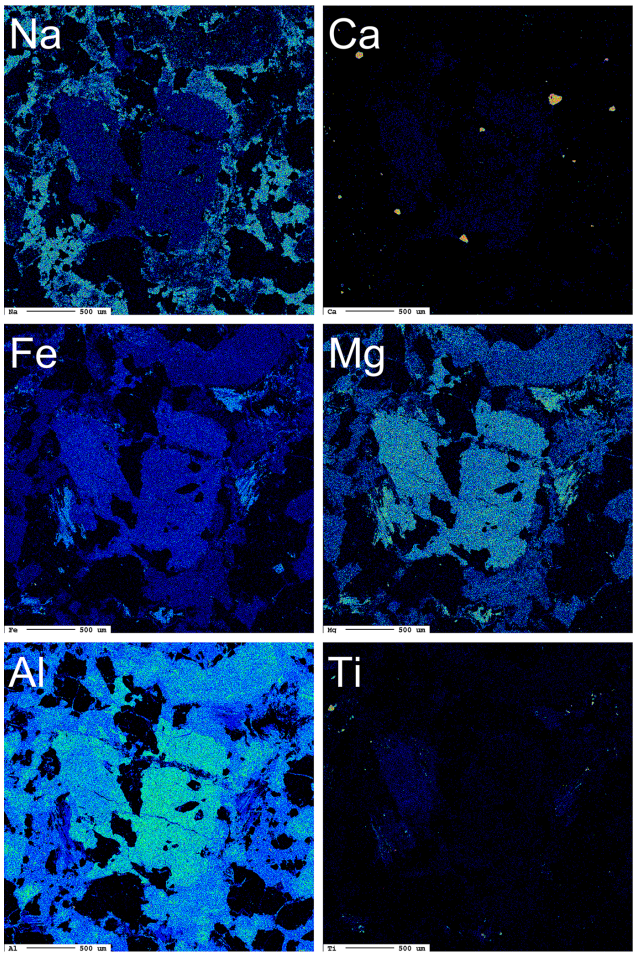

Figure 4. X-ray maps collected on dutrowite and associated oxy-dravite (see Fig. 1).

dravite. Refined unit-cell parameters are $a = 15.9544(2)$, $c = 7.1892(1)$ Å, and $V = 1584.80(5)$ Å^3. In agreement with the observed chemical variations, dutrowite has larger a, c, and V values, with $\Delta a = +0.2\,\%$, $\Delta c = +0.4\,\%$, and $\Delta V = +0.8\,\%$.

4.4 Genesis of dutrowite

Dutrowite occurs in the groundmass of the porphyritic metarhyolite belonging to the Fornovolasco Metarhyolite Formation. Actually, it was identified in an unusual sample, characterized by the presence of "biotite". This is a rare mineralogical feature of the Fornovolasco Metarhyolite, since the relics of "biotite" phenocrysts are usually completely replaced by Fe-rich clinochlore, quartz, and rutile (Vezzoni et al., 2018). Textural data indicating the relations of dutrowite with oxy-dravite are limited to a few observations, and the relations between these two phases are not clear. For instance, some zoned crystals, cut orthogonal to the c axis, show a Ti-enriched core (even if with Ti content < 0.25 apfu, i.e. not enough to classify the sample as dutrowite) and an oxy-dravitic rim (see Fig. 7 in Vezzoni et al., 2018). Although this texture might suggest that Ti-richer domains crystallized earlier, possibly at higher T, other tourmaline grains in the same specimen do not show such a regular zoning. For instance, the crystal in Fig. 1 is distinctly zoned, with a sector corresponding to oxy-dravite and the other in contact with "biotite" and partially replacing it. However, as usually occurs in relatively high-T late-magmatic/hydrothermal tourmalines in granitoid rocks, the mineral shows very complex, patchy zoning with no clear core-to-rim zoning.

As discussed above, "biotite" is a host for Ti in metarhyolite and may have played some role in the crystallization of dutrowite. Some authors (e.g. Dini et al., 2008; Gadas et al., 2019; Nabelek, 2021) stressed the role of this mica as a source of Ti for Ti-enriched tourmaline. Boron metasomatism and crystallization of tourmaline as a replacement of earlier magmatic silicates is well-known during the late-magmatic and early-hydrothermal evolution of several granitic intrusions (e.g. Woodford et al., 2001; Dini et al., 2008). These processes affected also the Fornovolasco Metarhyolite and could be related to the pre-Alpine tourmalinization and sericitization processes described by Vezzoni et al. (2020). Biotite from metarhyolite has $Mg/(Mg + Fe) = 0.39$, lower than that of both dutrowite (0.48) and oxy-dravite (0.54, ranging between 0.47 and 0.60). Consequently, some Fe could have been lost during the genesis of tourmaline, or it could have been fixed in pyrite, frequently occurring in metarhyolite. Preferential mobilization of Fe during the interaction between biotite and late-magmatic hydrothermal fluids is indicated by metasomatic tourmaline with a Mg content higher than that of the replaced biotite (Dini et al., 2008) as well as by hydrothermal experiments (Orlando et al., 2017). Moreover, the rather constant Ca content [$Ca/(Na + Ca) \sim 0.20$] in tourmaline could be sourced by plagioclase. Unfortunately, magmatic plagioclase is completely replaced by albite in the Fornovolasco Metarhyolite; however, a composition close to An_{20} is probable for the pristine plagioclase in this rock. The tourmalinization of magmatic silicates could also release SiO_2, favouring the formation of late-stage quartz veins in the metarhyolite and surrounding rocks.

Vereshchagin et al. (2022), on the basis of synthesis experiments, suggested that low-P conditions are favourable to Ti enrichment in tourmalines. As regards temperature conditions, a comparison with the Ti enrichment in other silicates can be proposed. For instance, "biotite" is enriched in Ti at low-P (as for tourmaline) and high-T (Henry et al., 2005). If so, dutrowite could be the result of the high-T/low-P replacement of "biotite" in the Fornovolasco Metarhyolite during the late-magmatic/hydrothermal evolution of this Permian intrusive rock.

The oxy-nature of both dutrowite and oxy-dravite does not necessarily imply an oxidizing geological environment, which would not be in accord with the local precipitation of pyrite and other sulfides in metarhyolite. As observed

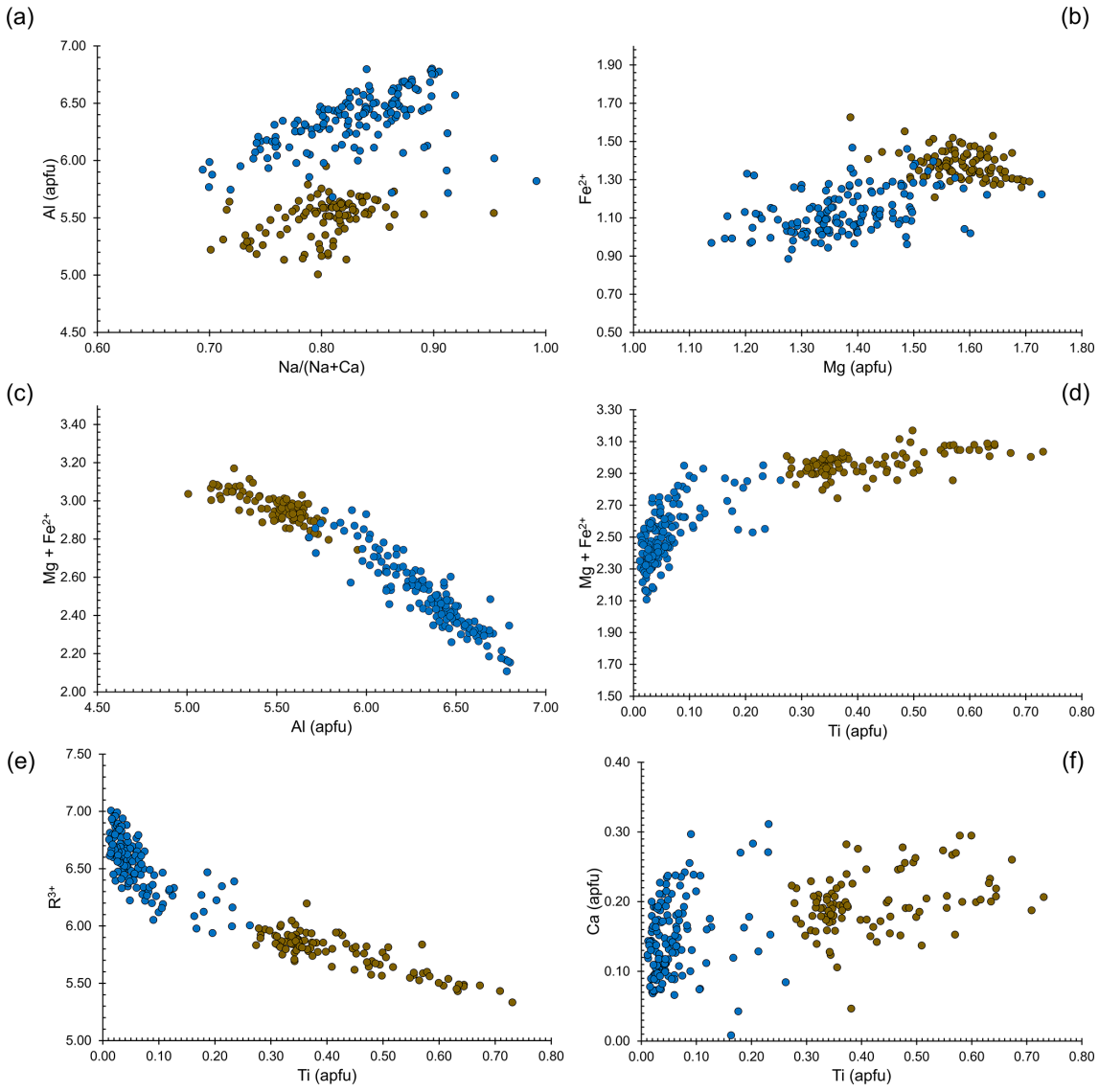

Figure 5. Relations between chemical constituents in dutrowite (brown circles) and associated oxy-dravite (blue circles).

in some oxy-tourmalines (e.g. Bačík et al., 2013), the deprotonization reaction could be simply due to local charge-balance requirements related to high-charged cations (e.g. Al^{3+}, Ti^{4+}), being the mineralogical expression of specific rock geochemistry.

5 Conclusion

Dutrowite is the first tourmaline supergroup mineral with Ti as a species-forming chemical constituent. Its finding and description improve the knowledge of the crystal chemistry of this important group of cyclosilicates and give some insights into the enrichment of Ti in these minerals, suggesting substitution mechanisms and the role of "biotite" as a source of Ti during the late-stage evolution of the magmatic–hydrothermal system associated with the emplacement of the Fornovolasco Metarhyolite Formation.

Available data also encourage a more accurate petrological study on this recently described geological formation (Pieruccioni et al., 2018), focusing on the tourmaline supergroup minerals, which show wide chemical variability. Their characterization may help in deciphering the evolution of this sector of the northern Apennines during both the Permian magmatic–hydrothermal history and the subsequent Alpine tectono-metamorphic events.

Data availability. The Crystallographic Information File data of dutrowite are available in the Supplement. Additional chemical data of dutrowite and associated oxy-dravite are also made available.

Supplement. The supplement related to this article is available online at: https://doi.org/10.5194/ejm-35-81-2023-supplement.

Author contributions. CB collected preliminary data. CB and DM carried out single-crystal X-ray diffraction and micro-Raman spectroscopy; CB and FB examined crystal–chemical data. FZ collected electron microprobe data. HS collected Mössbauer data. AD contributed to the geological background. CB, DM, and FB wrote the paper, with inputs from the other authors.

Competing interests. At least one of the (co-)authors is a member of the editorial board of *European Journal of Mineralogy*. The peer-review process was guided by an independent editor, and the authors also have no other competing interests to declare.

Disclaimer. Publisher's note: Copernicus Publications remains neutral with regard to jurisdictional claims in published maps and institutional affiliations.

Special issue statement. This article is part of the special issue "New minerals: EJM support". It is not associated with a conference.

Acknowledgements. Edward Grew is acknowledged for useful discussion. Yuri Galanti is thanked for field assistance during dutrowite sampling. The University Centrum for Applied Geosciences (UCAG) is thanked for the access to the E.F. Stumpfl electron microprobe laboratory. Frank Hawthorne and an anonymous reviewer are thanked for their comments.

Financial support. This research received support from the Ministero dell'Istruzione, dell'Università e della Ricerca through the project PRIN 2020 "HYDROX – HYDRous- vs. OXo-components in minerals: adding new pieces to the Earth's H_2O cycle puzzle" (project no. 2020WYL4NY). Ferdinando Bosi was supported by Sapienza University of Rome (Prog. Università 2020).

Review statement. This paper was edited by Sergey Krivovichev and reviewed by Frank Hawthorne and one anonymous referee.

References

Andreozzi, G. B., Bosi, F., and Longo, M.: Linking Mössbauer and structural parameters in elbaite-schorl-dravite tourmalines, Am. Mineral., 93, 658–666, 2008.

Armbruster, T., Bonazzi, P., Akasaka, M., Bermanec, V., Chopin, C., Gieré, R., Heuss-Assbichler, S., Liebscher, A., Menchetti, S., Pan, Y., and Pasero, M.: Recommended nomenclature of epidote-group minerals, Eur. J. Mineral., 18, 551–567, 2006.

Bačík, P., Cempírek, J., Uher, P., Novák, M., Ozdín, D., Filip, J., Škoda, R., Breiter, K., Klementová, M., Ďuda, R., and Groat, L. A.: Oxy-schorl, $Na(Fe^{2+}_2Al)Al_6Si_6O_{18}(BO_3)_3(OH)_3O$, a new mineral from Zlatá Idka, Slovak Republic and Přibyslavice, Czech Republic, Am. Mineral., 98, 485–492, 2013.

Bačík, P., Ozdín, D., Uher P., and Chovan, M.: Crystal chemistry and evolution of tourmaline in tourmalinites from Zlatá Idka, Slovakia, J. Geosci., 67, 209–222, 2022.

Bechi, E.: Intorno ad un nuovo minerale, Cont. Atti Accad. Georg. Firenze, 30, 84–87, 1852.

Benvenuti, M., Lattanzi, P., and Tanelli, G.: Tourmalinite-associated Pb-Zn-Ag mineralization at Bottino, Apuane Alps, Italy: geologic setting, mineral textures, and sulfide chemistry, Econ. Geol., 84, 1277–1292, 1989.

Benvenuti, M., Costagliola, P., Lattanzi, P., and Tanelli, G.: Mineral chemistry of tourmalines from the Bottino mining district, Apuane Alps (Italy), Eur. J. Mineral., 3, 537–548, 1991.

Biagioni, C., Mauro, D., and Pasero, M.: Sulfates from the pyrite ore deposits of the Apuan Alps (Tuscany, Italy): A review, Minerals, 10, 1092, https://doi.org/10.3390/min10121092, 2020.

Bonatti, S.: La roccia porfiroide di Forno Volasco, Atti Soc. Tosc. Sci. Nat. Mem., 43, 210–216, 1933.

Bosi, F.: Bond-valence constraints around the O1 site of tourmaline, Mineral. Mag., 77, 343–351, 2013.

Bosi, F. and Andreozzi, G. B.: A critical comment on Ertl et al. (2012): "Limitations of Fe^{2+} and Mn^{2+} site occupancy in tourmaline: Evidence from Fe^{2+}- and Mn^{2+}-rich tourmaline", Am. Mineral., 98, 2183–2192, 2013.

Bosi, F. and Skogby, H.: Oxy-dravite, $Na(Al_2Mg)(Al_5Mg)(Si_6O_{18})(BO_3)_3(OH)_3O$, a new mineral species of the tourmaline supergroup, Am. Mineral., 98, 1442–1448, 2013.

Bosi, F., Skogby, H., Lazor, P., and Reznitskii, L.: Atomic arrangements around the O3 site in Al- and Cr-rich oxy-tourmalines: a combined EMP, SREF, FTIR and Raman study, Phys. Chem. Miner., 42, 441–453, 2015.

Bosi, F., Biagioni, C., and Oberti, R.: On the chemical identification and classification of minerals, Minerals, 9, 591, https://doi.org/10.3390/min9100591, 2019.

Brese, N. E. and O'Keeffe, M.: Bond-valence parameters for solids, Acta Crystallogr. B, 47, 192–197, 1991.

Bruker AXS Inc.: APEX 3, Bruker Advanced X-ray Solutions, Madison, Wisconsin, USA, 2016.

da Fonseca-Zang, W. A., Zang, J. W., and Hofmeister, W.: The Ti-influence on the tourmaline color, J. Braz. Chem. Soc., 19, 1186–1192, 2008.

Dini, A., Mazzarini, F., Musumeci, G., and Rocchi, S.: Multiple hydro-fracturing by boron-rich fluids in the Late Miocene contact aureole of eastern Elba Island (Tuscany, Italy), Terra Nova, 20, 318–326, 2008.

Dottorini, V.: Cristallochimica di specie del supergruppo della tormalina dalla Toscana, thesis, University of Pisa, 283 pp., 2019.

Dutrow, B. and Henry, D.: Calcium-rich dravite from the Arignac Gypsum Mine, France: Implications for tourmaline development in a sulfate-rich, highly magnesian meta-evaporite, J. Geosci., 67, 191–207, 2022.

Flack, H. D.: On enantiomorph-polarity estimation, Acta Crystallogr. A, 39, 876–881, 1983.

Flégr, T., Novák, M., and Cempírek, J.: New occurrence of bosiite in the Řečice pegmatite, Czech Republic, in: New Minerals and Mineralogy in the 21st century, edited by: Gadas, P., International Scientific Symposium, Jáchymov, Minera Analytica, Prague, 23–25, 2016.

Gadas, P., Novák, M., Škoda, R., Cempírek, J., Zachař, A., Flégr, T., and Pezzotta, F.: Titanium in tourmalines from granitic pegmatites and their exocontacts, Can. Mineral., 57, 745–747, 2019.

Gasharova, B., Mihailova, B., and Konstantinov, L.: Raman spectra of various types of tourmaline, Eur. J. Mineral., 9, 935–940, 1997.

Gonzalez-Carreño, T., Fernandez, M., and Sanz, J.: Infrared and electron microprobe analysis in tourmalines, Phys. Chem. Miner., 15, 452–460, 1988.

Grice, J. D. and Ercit, T. S.: Ordering of Fe and Mg in the tourmaline crystal structure: the correct formula, Neues Jb. Miner. Monat., 165, 245–266, 1993.

Henry, D. and Dutrow, B: Metamorphic tourmaline and its petrologic applications, Rev. Mineral. Geochem., 33, 503–557, 1996.

Henry, D. J., Guidotti, C. V., and Thomson, J. A.: The Ti-saturation surface for low-to-medium pressure metapelitic biotites: Implications for geothermometry and Ti-substitution mechanisms, Am. Mineral., 90, 316–328, 2005.

Henry, D., Novák, M., Hawthorne, F. C., Ertl, A., Dutrow, B. L., Uher, P., and Pezzotta, F.: Nomenclature of the tourmaline-supergroup minerals, Am. Mineral., 96, 895–913, 2011.

Konzett, J., Krenn, K., Hauzenberger, C., Whitehouse, M., and Hoinkes, G.: High-pressure tourmaline formation and fluid activity in Fe–Ti-rich eclogites from the Kreuzeck Mountains, Eastern Alps, Austria, J. Petrol., 53, 99–125, 2012.

Kraus, W. and Nolze, G.: Powder Cell – a program for the representation and manipulation of crystal structures and calculation of the resulting X-ray powder patterns, J. Appl. Crystallogr., 29, 301–303, 1996.

Lottermoser, B. G. and Plimer, I. R.: Chemical variation in tourmalines, Umberatana, South Australia, Neues Jb. Miner. Monat., 7, 314–326, 1987.

Mandarino, J. A.: The Gladstone-Dale relationship. Part III. Some general applications, Can. Mineral., 17, 71–76, 1979.

Mandarino, J. A.: The Gladstone-Dale relationship. Part IV. The compatibility concept and some application, Can. Mineral., 19, 441–450, 1981.

Mauro, D., Biagioni, C., Hålenius, U., Skogby, H., Dottorini, V., and Bosi, F.: Nickel- and Fe^{3+}-rich oxy-dravite from the Artana Mn prospect, Apuan Alps (Tuscany, Italy), J. Geosci., 67, 141–150, 2022.

Nabelek, P. I.: Formation of metasomatic tourmalinites in reduced schists during the Black Hills orogeny, South Dakota, Am. Mineral., 106, 282–289, 2021.

Novák, M., Škoda, R., Filip, J., Macek, I., and Vaculovič, T.: Compositional trends in tourmaline from intragranitic NYF pegmatites of the Třebíč pluton, Czech Republic: an electron microprobe, Mössbauer and LA-ICP-MS study, Can. Mineral., 49, 359–380, 2011.

Orlandi, P. and Pasero, M.: Allanite-(La) from Buca della Vena mine, Apuan Alps, Italy, an epidote-group mineral, Can. Mineral., 44, 63–68, 2006.

Orlando, A., Ruggieri, G., Chiarantini, L., Montegrossi, G., and Rimondi, V.: Experimental Investigation of Biotite-Rich Schist Reacting with B-Bearing Fluids at Upper Crustal Conditions and Correlated Tourmaline Formation, Minerals, 7, 155, https://doi.org/10.3390/min7090155, 2017.

Paoli, G., Stokke, H. H., Rocchi, S., Sirevaag, H., Ksienzyk, A. K., Jacobs, J., and Košler, J.: Basement provenance revealed by U-Pb detrital zircon ages: a tale of African and European heritage in Tuscany, Italy, Lithos, 277, 376–387, 2017.

Pesquera, A., Gil-Crespo, P. P., Torres-Ruiz, F., Torres-Ruiz, J., and Roda-Robles, E.: A multiple regression method for estimating Li in tourmaline from electron microprobe analyses, Mineral. Mag., 80, 1129–1133, 2016.

Pieruccioni, D., Galanti, Y., Biagioni, C., and Molli, G.: The geological map of the Fornovolasco area, Apuan Alps (Tuscany, Italy), J. Maps, 14, 357–367, 2018.

Povondra, P.: The crystal chemistry of tourmalines of the schorl-dravite series, Acta U. Carol. Geol., 3, 223–264, 1981.

Prescher, C., McCammon, C., and Dubrovinsky, L.: MossA: a program for analyzing energy-domain Mössbauer spectra from conventional and synchrotron sources, J. Appl. Crystallogr., 45, 329–331, 2012.

Ribeiro da Costa, I., Ribeiro Antunes, I. M. H., and Récio, C.: The $Mg/(Fe + Mg)$ ratio and the Ti and A site contents of tourmaline as promising indicators of granitic magma evolution, J. Iber. Geol., 47, 307–321, 2021.

Rossman, G. R. and Mattson, S. M.: Yellow, Mn-rich elbaite with Mn-Ti intervalence charge-transfer, Am. Mineral., 71, 599–602, 1986.

Scribner, E. D., Groat, L. A., and Cempírek, J.: Mineralogy of Ti-bearing, Al-deficient tourmaline assemblages associated with lamprophyre dikes near the O'Grady Batholith, Northwest Territories, Canada, J. Geosci., 63, 123–135, 2018.

Shannon, R. D.: Revised effective ionic radii and systematic studies of interatomic distances in halides and chalcogenides, Acta Crystallogr. A, 32, 751–767, 1976.

Sheldrick, G. M.: Crystal structure refinement with SHELXL, Acta Crystallogr. C, 71, 3–8, 2015.

Vereshchagin, O. S., Wunder, B., Baksheev, I. A., Wilke, F. D. H., Vlasenko, N. S., and Frank-Kamenetskaya, O.: Ti^{4+} and Sn^{4+}-bearing tourmalines – pressure control and comparison of synthetic and natural counterparts, J. Geosci., 67, 163–171, 2022.

Vezzoni, S., Biagioni, C., D'Orazio, M., Pieruccioni, D., Galanti, Y., Petrelli, M., and Molli, G.: Evidence of Permian magmatism in the Alpi Apuane metamorphic complex (Northern Apennines, Italy): New hints for the geological evolution of the basement of the Adria plate, Lithos, 318–319, 104–123, 2018.

Vezzoni, S., Pieruccioni, D., Galanti, Y., Biagioni, C., and Dini, A.: Permian hydrothermal alteration preserved in polymetamorphic basement and constraints for ore-genesis (Alpi Apuane, Italy), Geosciences, 10, 399, https://doi.org/10.3390/geosciences10100399, 2020.

Warr, L. N.: IMA-CNMNC approved mineral symbols, Mineral. Mag., 85, 291–320, 2021.

Watenphul, A., Burgdorf, M., Schlüter, J., Horn, I., Malcherek, T., and Mihailova, B.: Exploring the potential of Raman spectroscopy for crystallochemical analyses of complex hydrous silicates: II. Tourmalines, Am. Mineral., 101, 970–985, 2016a.

Watenphul, A., Schlüter, J., Bosi, F., Skogby, H., Malcherek, T., and Mihailova, B.: Influence of the octahedral cationic-site occupancies on the framework vibrations of Li-free tourmalines, with im-

plications for estimating temperature and oxygen fugacity in host rocks, Am. Mineral., 101, 2554–2563, 2016b.

Wilson, A. J. C. (Ed.): International Tables for Crystallography Volume C: Mathematical, Physical and Chemical Tables, Kluwer Academic Publishers, Dordrecht, the Netherlands, 1992.

Wojdyr, M.: Fityk: a general-purpose peak fitting program, J. Appl. Crystallogr., 43, 1126–1128, 2010.

Woodford, D. T., Sisson, V. B., and Leeman, W. P.: Boron metasomatism of the Alta stock contact aureole, Utah: evidence from borates, mineral chemistry and geochemistry, Am. Mineral., 86, 513–533, 2001.

Wright, S. E., Foley, J. A., and Hughes, J. M.: Optimization of site occupancies in minerals using quadratic programming, Am. Mineral., 85, 524–531, 2000.

Žáček, V., Frýda, J., Petrov, A., and Hyršl, J.: Tourmalines of the povondraite – (oxy)dravite series from the cap rock of metaevaporite in Alto Chapare, Cochacamba, Bolivia, J. Czech Geol. Soc., 45, 3–12, 2000.